

Magnetism as a Mass Term of the Edge States in Graphene

Ken-ichi SASAKI^{1,2*} and Riichiro SAITO^{1,2}

¹*Department of Physics, Tohoku University, Sendai 980-8578*

²*CREST, Japan Science and Technology Agency, Sendai 980-8578*

(Received January 28, 2008; accepted February 26, 2008; published April 25, 2008)

The magnetism by the edge states in graphene is investigated theoretically. An instability of the pseudo-spin order of the edge states induces ferrimagnetic order in the presence of the Coulomb interaction. Although the next nearest-neighbor hopping can stabilize the pseudo-spin order, a strong Coulomb interaction makes the pseudo-spin unpolarized and real spin polarized. The magnetism of the edge states makes two peaks of the density of states in the conduction and valence energy bands near the Fermi point. Using a continuous model of the Weyl equation, we show that the edge-induced gauge field and the spin dependent mass terms are keys to make the magnetism of the edge states. A relationship between the magnetism of the edge states and the parity anomaly is discussed.

KEYWORDS: graphene, edge state, magnetism, Coulomb interaction, Weyl equation, gauge field, mass term, parity anomaly

DOI: [10.1143/JPSJ.77.054703](https://doi.org/10.1143/JPSJ.77.054703)

1. Introduction

The electronic properties of graphene^{1–3)} have attracted much attention mainly because of its relativistic character of low energy electronic excitation. The energy band structure of graphene consists of two Dirac cones at the K and K' points in the k -space. The electron dynamics around each Dirac point is approximated by the Weyl equation which describes a massless particle. When we consider solutions of the Weyl equation for a finite (or semi-finite) graphene cluster (ribbon) with the zigzag edges, the spatially-localized edge states⁴⁾ exist around the Fermi energy.⁵⁾ The existence of the edge states depends on the shape of the edge for a graphene cluster. For example, the zigzag edge yields the edge states while the armchair edge does not. The energy dispersion for the edge states which appears only between the two Dirac points smoothly connects to the energy dispersion of the delocalized states.⁶⁾ A large local density of states (LDOS) by the edge states may induce magnetism⁴⁾ and superconductivity⁷⁾ near the zigzag edge. The existence of a mass for the Dirac particle is an important issue because it gives rise to an energy gap at the Dirac points and relates to the ordered states. We examine a mechanism that the Coulomb interaction makes a mass and a magnetism.

Fujita *et al.* discussed the effect of the Coulomb interaction on the edge state, in which the electronic spins are localized at the edge to form a ferromagnetic state at one zigzag edge and another ferromagnetic state with the opposite spin at another zigzag edge.⁴⁾ The occurrence of the magnetism is investigated by first principles calculations, too.^{8–10)} If the ferromagnetic state appeared at one edge, we would expect that two peaks for up and down spin states appear in scanning tunneling spectroscopy (STS). However this situation seems to be inconsistent with the STS measurements in which they observed only one LDOS peak near the zigzag edge of graphite.^{11–15)} Klusek *et al.*¹¹⁾ found a peak of LDOS in the energy range of 20–250 meV above the Fermi level at the edges of circular pits on graphite surface. Kobayashi *et al.*^{12,13)} and Niimi *et al.*^{14,15)} independently observed a peak in the LDOS below the Fermi

energy by 20–30 meV. Since the peak appears only conduction (Klusek *et al.*) or valence energy band (Kobayashi *et al.* and Niimi *et al.*), it suggests that the edge states do not make a magnetism. Thus it is an interesting problem for understanding the occurrence of the ferromagnetic order at the edge in the presence of the Coulomb interaction. When we see the calculated results of Fujita *et al.*, the polarized spin appears for the edge states at a much small on-site Coulomb interaction U value compared with the nearest neighbor interaction γ_0 (see Fig. 5 in ref. 4). Although we reproduce their results numerically, the results are very surprising. A possible reason why the spin ordering occurs for such a small U is due to a special fact that the wavefunction of the edge states has an amplitude only one of the two sublattices (A and B) and thus the nearest neighbor interaction is suppressed. When we introduce the next nearest neighbor interaction, γ_n , the spin polarization around $U/\gamma_0 \sim 0$ disappears and spin ordering appears from finite values of U depending on γ_n , which we will show in this paper.

The wavefunction for two sublattice structure is referred to as the “pseudo-spin”. An edge state can be described by a pseudo-spin polarized state.⁶⁾ A pseudo-spin structure gives a rich variety of interesting physical phenomena not only the edge states but also the extended states. For example, the absence of backward scattering mechanism is relevant to this pseudo-spin nature,^{16,17)} in which a 2π rotation of a pseudo-spin wavefunction around the K-point in the two-dimensional Brillouin zone does not give the original wavefunction but gives minus sign to the wavefunction. Thus, the pseudo-spin is quite similar to the real spin in the real space. In this paper, we show that the pseudo-spin also plays an important role for the magnetism (or real spin) of the edge states, which is shown by a numerical analysis of the lattice model and by an analytical study of the Weyl equation.

This paper is organized as follows. In §2 we explain the model Hamiltonian and introduce symmetric and antisymmetric variables for the pseudo-spin. In §3 we show numerical results for the ground state of the model. In §4 we use a continuous model to examine the mechanism of the magnetism of the edge states. Discussion and summary are given in §5.

*E-mail: sasaken@flex.phys.tohoku.ac.jp

2. Pseudo-Spin Representation of Hamiltonian

The Hamiltonian is given by $\mathcal{H}_{0\uparrow} + \mathcal{H}_{0\downarrow} + \mathcal{H}_U$ where $\mathcal{H}_{0s} \equiv -\gamma_0 \sum_{\langle i,j \rangle} c_{s,i}^\dagger c_{s,j}$ ($s = \uparrow, \downarrow$) is the nearest-neighbor tight-binding Hamiltonian ($\gamma_0 \approx 3$ eV is the hopping integral), and \mathcal{H}_U is the Hubbard on-site interaction. \mathcal{H}_U is written as

$$\mathcal{H}_U = U \sum_{\mathbf{r}} n_{\uparrow}(\mathbf{r}) n_{\downarrow}(\mathbf{r}), \quad (1)$$

where U is the on-site energy and $n_{\uparrow}(\mathbf{r})$ ($n_{\downarrow}(\mathbf{r})$) is the density operator of up (down) spin electron at site \mathbf{r} . Since the hexagonal lattice consists of two sublattices, A and B, \mathcal{H}_U is given as a summation over unit cells as

$$\mathcal{H}_U = U \sum_{\mathbf{r}_u} \sum_{p=A,B} n_{\uparrow,p}(\mathbf{r}_u) n_{\downarrow,p}(\mathbf{r}_u), \quad (2)$$

where $n_{\uparrow,p}(\mathbf{r}_u)$ ($n_{\downarrow,p}(\mathbf{r}_u)$) is the density operator of up (down) spin electron at p -sublattice ($p = A, B$), and \mathbf{r}_u denotes the position of a unit cell. For a unit cell, we introduce a density and a magnetization at \mathbf{r}_u as $n_p(\mathbf{r}_u) = n_{\uparrow,p}(\mathbf{r}_u) + n_{\downarrow,p}(\mathbf{r}_u)$ and $m_p(\mathbf{r}_u) = n_{\uparrow,p}(\mathbf{r}_u) - n_{\downarrow,p}(\mathbf{r}_u)$, respectively. Hereafter \mathbf{r}_u for each variable is omitted for simplicity. From n_p and m_p , we define density and magnetization for a unit cell as

$$n = n_A + n_B, \quad m = m_A + m_B. \quad (3)$$

n and m are symmetric with respect to the sublattice. Here we introduce pseudospin order and antiferromagnetic order for a unit cell,

$$p_n = n_A - n_B, \quad p_m = m_A - m_B, \quad (4)$$

which are anti-symmetric with respect to the sublattice. p_n (p_m) represents charge (spin) polarization within the hexagonal unit cell. \mathcal{H}_U can be rewritten in terms of $n, m, p_n,$ and p_m as

$$\mathcal{H}_U = \frac{U}{8} \sum_{\mathbf{r}_u} (n^2 + p_n^2 - m^2 - p_m^2). \quad (5)$$

This representation of \mathcal{H}_U shows that not only non-vanishing magnetization ($\langle m \rangle \neq 0$) but also antiferromagnetic ($\langle m \rangle = 0$ and $\langle p_m \rangle \neq 0$) or ferrimagnetic ($\langle m \rangle \neq 0$ and $\langle p_m \rangle \neq 0$) spin configuration are favored to decrease \mathcal{H}_U where $\langle \mathcal{O} \rangle$ denotes the expectation value of operator \mathcal{O} for the ground state.

By applying the mean-field approximation to eq. (2), $\mathcal{H}_U = U \sum_{\mathbf{r}_u,p} \langle n_{\uparrow,p} \rangle n_{\downarrow,p} + n_{\uparrow,p} \langle n_{\downarrow,p} \rangle - \langle n_{\uparrow,p} \rangle \langle n_{\downarrow,p} \rangle$, the Hamiltonians for up and down spin electrons in graphene are given as follows:

$$\begin{aligned} \mathcal{H}_{\uparrow} &\equiv \mathcal{H}_{0\uparrow} + \frac{U}{2} \sum_{\mathbf{r}_u} \begin{pmatrix} \langle n_A - m_A \rangle & 0 \\ 0 & \langle n_B - m_B \rangle \end{pmatrix} \begin{pmatrix} n_{\uparrow,A} \\ n_{\uparrow,B} \end{pmatrix}, \\ \mathcal{H}_{\downarrow} &\equiv \mathcal{H}_{0\downarrow} + \frac{U}{2} \sum_{\mathbf{r}_u} \begin{pmatrix} \langle n_A + m_A \rangle & 0 \\ 0 & \langle n_B + m_B \rangle \end{pmatrix} \begin{pmatrix} n_{\downarrow,A} \\ n_{\downarrow,B} \end{pmatrix}. \end{aligned} \quad (6)$$

The Hamiltonians of eq. (6) can also be rewritten using eqs. (3) and (4) as

$$\begin{aligned} \mathcal{H}_{\uparrow} &= \mathcal{H}_{0\uparrow} + \frac{U}{4} \sum_{\mathbf{r}_u} [(\langle p_n \rangle - \langle p_m \rangle) \sigma_z + (\langle n \rangle - \langle m \rangle) I] \begin{pmatrix} n_{\uparrow,A} \\ n_{\uparrow,B} \end{pmatrix}, \\ \mathcal{H}_{\downarrow} &= \mathcal{H}_{0\downarrow} + \frac{U}{4} \sum_{\mathbf{r}_u} [(\langle p_n \rangle + \langle p_m \rangle) \sigma_z + (\langle n \rangle + \langle m \rangle) I] \begin{pmatrix} n_{\downarrow,A} \\ n_{\downarrow,B} \end{pmatrix}, \end{aligned} \quad (7)$$

Table I. Parities with respect to spin and pseudo-spin.

	p_n	p_m	n	m	σ_z	Coupling
Spin ($\uparrow \leftrightarrow \downarrow$)	+	-	+	-	+	\mathbf{B}^{em}
Pseudo-spin ($A \leftrightarrow B$)	-	-	+	+	-	\mathbf{B}^{q}

where $\sigma_z = \text{diag}(1, -1)$ and $I = \text{diag}(1, 1)$. The pseudo-spin variables are proportional to σ_z and affect magnetization of the edge states as we will show in the following sections.

In Table I, we show the parities of $p_n, p_m, n, m,$ and σ_z for changing the direction of spin and pseudo-spin. The interaction terms in eq. (7) are invariant with respect to pseudo-spin parity: $p_n \rightarrow -p_n, p_m \rightarrow -p_m, n \rightarrow n, m \rightarrow m,$ and $\sigma_z \rightarrow -\sigma_z$, and we have $\mathcal{H}_{\uparrow} \leftrightarrow \mathcal{H}_{\downarrow}$ for spin parity: $p_n \rightarrow p_n, p_m \rightarrow -p_m, n \rightarrow n, m \rightarrow -m,$ and $\sigma_z \rightarrow \sigma_z$. Since \mathcal{H}_U is even parity with respect to spin and pseudo-spin, it is expected that a ground state is realized by spontaneous symmetry breaking if $\mathcal{H}_{0\uparrow} + \mathcal{H}_{0\downarrow}$ ($\equiv \mathcal{H}_0$) is symmetric, too. \mathcal{H}_0 is symmetric with respect to spin but asymmetric with respect to pseudo-spin due to the presence of the zigzag boundary. This can be explained as follows. A magnetic field, $\mathbf{B}^{\text{em}}(\mathbf{r})$, breaks the spin degeneracy of the ground state by the Zeeman term, $-\mathbf{B}^{\text{em}}(\mathbf{r}) \cdot \mathbf{m}(\mathbf{r})$, which is odd parity with respect to spin. Similarly, we can define a pseudo-magnetic field, $\mathbf{B}^{\text{q}}(\mathbf{r})$, that couples to σ_z and breaks the degeneracy of the pseudo-spin parity. $\mathbf{B}^{\text{q}}(\mathbf{r})$ is defined by the rotation of a deformation-induced gauge field $\mathbf{A}^{\text{q}}(\mathbf{r})$ as $\mathbf{B}^{\text{q}}(\mathbf{r}) = \nabla \times \mathbf{A}^{\text{q}}(\mathbf{r})$,¹⁸ which is similar to that $\mathbf{B}^{\text{em}}(\mathbf{r})$ is given by the rotation of an electro-magnetic gauge field $\mathbf{A}^{\text{em}}(\mathbf{r})$.

In the previous paper, we derived $\mathbf{A}^{\text{q}}(\mathbf{r})$ and $B_z^{\text{q}}(\mathbf{r})$ for zigzag edges.⁵ $\mathbf{A}^{\text{q}}(\mathbf{r})$ is given by a small change of the hopping integral from $-\gamma_0$ between an A-atom and one of the nearest B-atoms [$\delta\gamma_a(\mathbf{r})$ where $a = 1, 2, 3$, see Fig. 1] as

$$\begin{aligned} v_{\text{F}} A_x^{\text{q}}(\mathbf{r}) &= \delta\gamma_1(\mathbf{r}) - \frac{1}{2}(\delta\gamma_2(\mathbf{r}) + \delta\gamma_3(\mathbf{r})), \\ v_{\text{F}} A_y^{\text{q}}(\mathbf{r}) &= \frac{\sqrt{3}}{2}(\delta\gamma_2(\mathbf{r}) - \delta\gamma_3(\mathbf{r})). \end{aligned} \quad (8)$$

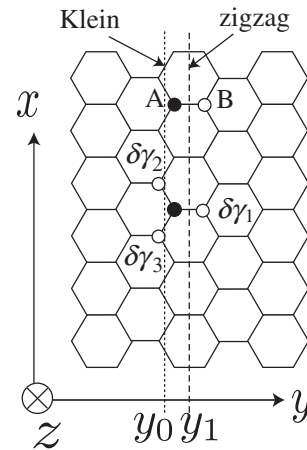


Fig. 1. Local modulation of the hopping integral is defined by $\delta\gamma_a$ ($a = 1, 2, 3$), which is related to $\mathbf{A}^{\text{q}}(\mathbf{r})$ through eq. (8). When we cut the bonds on the dashed (dotted) line by setting $\delta\gamma_1 = \gamma_0$ and $\delta\gamma_2 = \delta\gamma_3 = 0$ ($\delta\gamma_1 = 0$ and $\delta\gamma_2 = \delta\gamma_3 = \gamma_0$), we obtain the zigzag (Klein) edge.

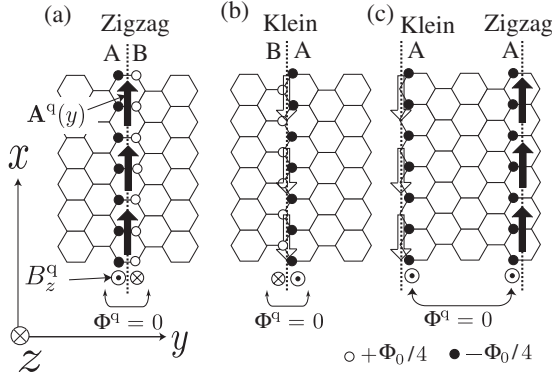


Fig. 2. Configuration of $A^q(\mathbf{r})$ and $B_z^q(\mathbf{r})$ for (a) the zigzag edge and (b) the Klein edge. When we cut the graphene sheet at the dashed line, the edge and $A^q(\mathbf{r}) = (A_x^q(y), 0)$ appears. The direction of $A^q(\mathbf{r})$ for the Klein edge is opposite to that of the zigzag edge. (c) A graphene with the zigzag edge and the Klein edge.

When we cut the bonds on the dashed line at y_1 in Fig. 1, we get a zigzag edge, while we get a Klein edge^{19,20} for the dotted line at y_0 . In the case of the zigzag edge, since $\delta\gamma_1(y) \neq 0$ and $\delta\gamma_2(\mathbf{r}) = \delta\gamma_3(\mathbf{r}) = 0$, we get $v_F A_x^q(y) = \delta\gamma_1(y) (> 0)$ and $v_F A_y^q = 0$, and thus, $B_z^q(\mathbf{r}) = -\partial_y A_x^q(y)$ as shown in Fig. 2(a). On the other hand, in the case of the Klein edge, since $\delta\gamma_1(\mathbf{r}) = 0$ and $\delta\gamma_2(y) = \delta\gamma_3(y) \neq 0$, we get $v_F A_x^q(y) = -\delta\gamma_2(y) (< 0)$ and $v_F A_y^q = 0$, and thus, $B_z^q(\mathbf{r}) = -\partial_y A_x^q(y)$ as shown in Fig. 2(b). The directions of $A^q(\mathbf{r})$ and $B^q(\mathbf{r})$ for the Klein edge are opposite to those for the zigzag edge [Figs. 2(a) and 2(b)]. Kusakabe and Maruyama discussed the edge state magnetism for a graphene cluster with a zigzag edge at one edge and a Klein edge at another edge,⁹ as shown in Fig. 2(c). In all cases, we can explain the edge structure within the same frame.

Since $B_z^q(\mathbf{r}) = -\partial_y A_x^q(y)$ appears at the zigzag edge,⁵ \mathcal{H}_0 can induce a pseudo-spin order, $\langle p_n \rangle \neq 0$, near the edge. In the next section, we will show numerically that \mathcal{H}_0 of a zigzag nanotube breaks the pseudo-spin parity of p_n , which is important to obtain magnetism for the total Hamiltonian, $\mathcal{H}_\uparrow + \mathcal{H}_\downarrow$.

3. Numerical Results and Analysis

In this section, we show numerical results for the ground state of the mean-field Hamiltonian $\mathcal{H}_\uparrow + \mathcal{H}_\downarrow$ in eq. (6). $\langle n/4 \rangle$, $\langle p_n \rangle$, $\langle p_m \rangle$, and $\langle m \rangle$ are plotted for (50, 0) zigzag nanotube with length $L \approx 4$ nm, and LDOS curves are calculated for (100, 0) zigzag nanotube with length $L \approx 20$ nm. Here (50, 0) (or (100, 0)) is the chiral index of a zigzag nanotube.²¹ We set the origin of the Fermi energy $E_F = 0$ as $\mathcal{H}_s = U/2$.

In Fig. 3(a), we plot $\langle n/4 \rangle$ and $\langle p_n \rangle$ in the case of $U = 0$. Since $U = 0$, $\langle m \rangle = \langle p_m \rangle = 0$. The solid (dashed) curves are the results for the Fermi energy $E_F = -0.01$ eV (+0.01 eV). $\langle n/4 \rangle$ and $\langle p_n \rangle$ are modulated near the edges and their difference from the constant values ($\langle n/4 \rangle = 0.5$ and $\langle p_n \rangle = 0$) is due to the presence of the edge states.⁴ The wavefunction of the edge states is localized near the edges so that $\langle n/4 \rangle$ is different from 0.5 (i.e., half filling $n = 2$) only near the edges. Moreover, the wavefunction of the edge states is polarized about the pseudo-spin and $\langle p_n \rangle$ is nonzero, too. $\langle n/4 \rangle$ and $\langle p_n \rangle$ are unstable against a small change of E_F due

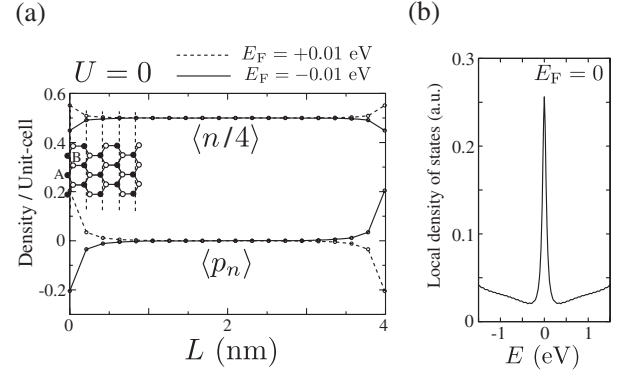


Fig. 3. (a) Self-consistent solution of $\langle n/4 \rangle$ and $\langle p_n \rangle$ for $U = 0$ and $E_F = \pm 0.01$ eV. Due to the presence of the edge states consisting a flat energy band at $E_F = 0$, $\langle n/4 \rangle$ and $\langle p_n \rangle$ are unstable against the small change of E_F . $\langle \mathcal{O}(\mathbf{r}_u) \rangle$ depends only on the distance from an edge due to rotational symmetry around the axis of the tube. (b) Corresponding LDOS curve at $L \approx 0.5$ nm. The degenerate spin up and down edge states make a sharp peak at $E_F = 0$ in the case of $U = 0$.

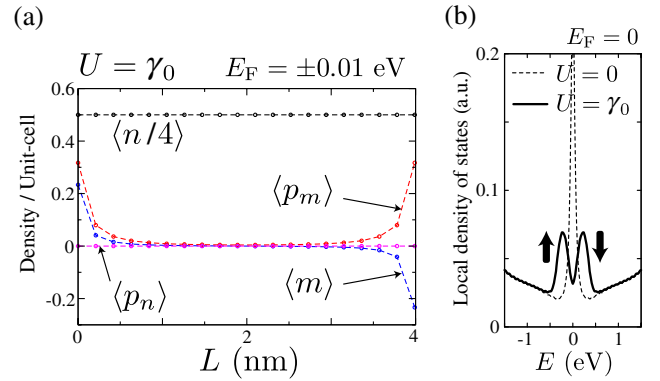


Fig. 4. (Color online) (a) Self-consistent solution of $\langle n/4 \rangle$, $\langle m \rangle$, $\langle p_n \rangle$, and $\langle p_m \rangle$ for $U = \gamma_0$ and $E_F = \pm 0.01$ eV. The spin around the edge is polarized and $|\langle p_m \rangle| \approx |\langle m \rangle|$ shows that spin is a ferrimagnetic configuration. (b) The LDOS curve at $L \approx 0.5$ nm shows that spin up edge states (denoted by up-arrow) and spin down edge states (denoted by down-arrow) make two sharp peaks (solid curve) near $E_F = 0$ when $U \neq 0$.

to the flat energy band of the edge states. In Fig. 3(b), we plot the LDOS at $L \approx 0.5$ nm in the case of $E_F = 0$. The spin up edge states and spin down edge states are degenerate in the case of $U = 0$ so that they make a sharp LDOS peak at $E_F = 0$. To show the (smooth) LDOS curve, we put a constant width (0.05 eV) for each state.

In Fig. 4(a), we plot self-consistent solution of $\langle n/4 \rangle$, $\langle m \rangle$, $\langle p_n \rangle$, and $\langle p_m \rangle$ in the case of $U = \gamma_0$. The result shows that, $\langle n/4 \rangle \approx 0.5$ and $\langle p_n \rangle \approx 0$ hold at each hexagonal unit cell, and $\langle m \rangle$ and $\langle p_m \rangle$ become nonzero near the zigzag edges. Since \mathcal{H}_U can stabilize $\langle n \rangle$ and $\langle p_n \rangle$ according to eq. (5), the pseudo-spin polarization ($\langle p_n \rangle \neq 0$) which exists for $U = 0$ disappears for the ground state due to a finite value of U . The corresponding LDOS curve is shown in Fig. 4(b). Because of U , the spin up (down) edge states are shifted above (below) the Fermi energy so that the ferrimagnetic order ($\langle m \rangle \neq 0$ and $\langle p_m \rangle \neq 0$) appears and that two LDOS peaks appear around $E_F = 0$. The LDOS curve in the case of $U = 0$ is also shown in Fig. 4(b) for comparison.

The numerical results can be explained qualitatively using eq. (7) as follows. When $\langle p_n \rangle = 0$ and $\langle p_m \rangle > 0$, the energy

of a spin up electron is shifted below the Fermi energy for a pseudo-spin up state ($\sigma_z = 1$). On the other hand, the energy of a spin down electron is shifted above the Fermi energy for the same state (a pseudo-spin up state). Thus, when $E_F = 0$, the ground state has a finite positive value of $\langle p_m \rangle$ and $\langle m \rangle$, which lowers the energy of a spin up electron due to the last term in eq. (7) and stabilizes the ground state configuration further. In fact, the second terms of the right-hand side of eq. (7) give rise to an energy gap in the energy spectrum. As we will show using a continuous model for \mathcal{H}_{0s} in §4, the appearance of the gap will become more clear since the term proportional to σ_z acts as a mass term of Dirac fermion. It is noted that $\langle p_n \rangle = 0$ is consistent with the presence of a gap, and non-vanishing $\langle p_m \rangle$ gives different signs of the mass terms for spin up and down electrons.

Next, we consider the next-nearest neighbor (nnn) hopping, γ_n , which is an intrinsic perturbation to the edge states. In the previous paper, we showed that the nnn interaction, \mathcal{H}_{nnn} , gives a finite energy bandwidth to the edge states, $W = \gamma_n$.²²⁾ $\gamma_n \approx 0.1\gamma_0$ is obtained by first-principles calculation using the local density approximation.²³⁾ A finite energy band width of the edge states suppresses the above mentioned $\langle p_n \rangle$'s instability with respect to a small change of E_F (see Fig. 3).

To see the relationship between $\langle p_n \rangle$ and $\langle p_m \rangle$ in detail, we first define the net pseudo-spin order P_n and the averaged antiferromagnetic order P_m : $P_n \equiv \sum_u \langle p_n(\mathbf{r}_u) \rangle / n$ and $P_m \equiv \sum_u \langle p_m(\mathbf{r}_u) \rangle / n$ where the summation is taken over all hexagonal unit cells. Since not only the edge states but also extended states can contribute to P_i ($i = n, m$), we consider the difference between P_i for a tube with the zigzag edges (P_i^{tube}) and that for a corresponding periodic torus system (P_i^{torus}) which does not have edge. $P_m^{\text{edge}} \equiv P_m^{\text{tube}} - P_m^{\text{torus}}$ can be used to show the magnetism for the edge states.

In Fig. 5(a), we plot P_m^{edge} (solid curve) and P_n^{edge} (dashed curve) as a function of U/γ_0 for $\gamma_n = 0$ (black), $0.1\gamma_0$ (red), and $0.2\gamma_0$ (blue). When $\gamma_n = 0$, no pseudo-spin order $P_n^{\text{edge}} \approx 0$ for any positive value of U , while the antiferromagnetic order P_m^{edge} increases until $U/\gamma_0 \approx 2.1$. P_m^{edge} decreases when $U/\gamma_0 > 2.1$. However Fujita *et al.* showed that the magnetism due to the extended states increases.⁴⁾ In case of a finite value of γ_n , the antiferromagnetic order is suppressed $P_m^{\text{edge}} \approx 0$ up to a finite value of U and the magnetism (in the case of $\gamma_n = 0$) appears discontinuously above the critical value of U . On the other hand, the pseudo-spin order appears $P_n^{\text{edge}} \neq 0$ below the critical value of U . Thus, when $E_F = 0$, we see that γ_n controls the occurrence of the pseudo-spin order (P_n^{edge}) and the antiferromagnetic order (P_m^{edge}) exclusively. In Fig. 5(b), we plot the LDOS curves when $U = \gamma_0$ for $\gamma_n = 0.1\gamma_0$ (solid curve) and $\gamma_n = 0.2\gamma_0$ (dashed curve). When $\gamma_n = 0.1\gamma_0$, magnetic order is realized so that there are two peaks in the LDOS curve. When $\gamma_n = 0.2\gamma_0$, the pseudo-spin order P_n^{edge} is realized and there is one peak below the Fermi energy in the LDOS curve. In the case of $U = 0$, the peak position appears at $E = -\gamma_n$.²²⁾ The pseudo-spin order shifts the peak position above $E = -\gamma_n$ due to $(U/4) \sum_{\mathbf{r}_u} \langle p_n \rangle \sigma_z$ in eq. (7). This is a possible reason why Kobayashi *et al.*^{12,13)} and Niimi *et al.*^{14,15)} observed a peak in the LDOS below the Fermi energy by 20–30 meV not by $\gamma_n \approx 0.3$ eV.²³⁾ Since the most

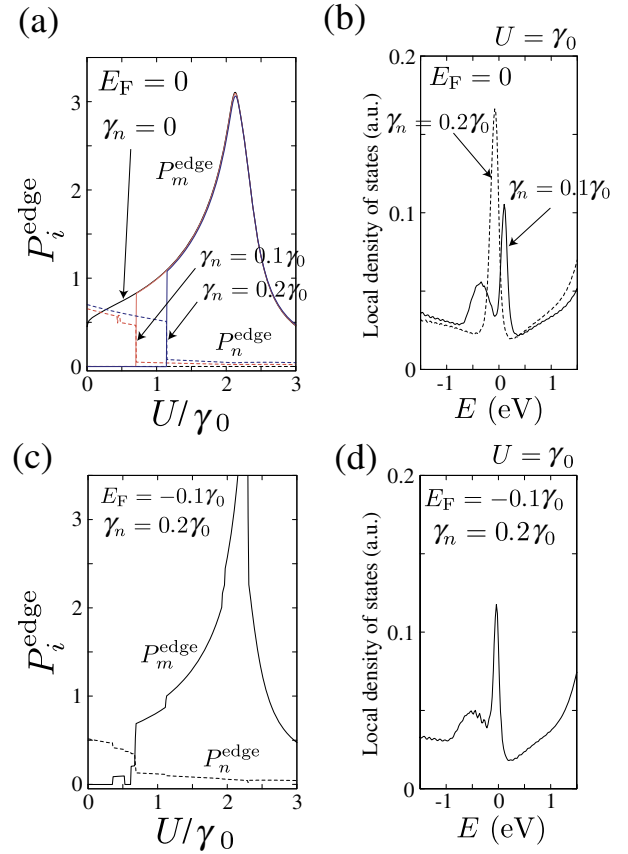


Fig. 5. (Color online) (a) Self-consistent solution of P_m^{edge} (solid curve) and P_n^{edge} (dashed curve) as a function of U/γ_0 for $\gamma_n = 0$ (black), $0.1\gamma_0$ (red), and $0.2\gamma_0$ (blue) in the case of $E_F = 0$. γ_n controls the appearance of the pseudo-spin order (P_n^{edge}) and of the ferrimagnetic order (P_m^{edge}). (b) The LDOS curves for $\gamma_n = 0.1\gamma_0$ (solid curve) and $\gamma_n = 0.2\gamma_0$ (dashed curve) when $U = \gamma_0$ and $E_F = 0$. (c) P_m^{edge} (solid curve) and P_n^{edge} (dashed curve) for $\gamma_n = 0.2\gamma_0$ with $E_F = -0.1\gamma_0$. This corresponds to that E_F is located at the center of the edge energy band. The small step on P_m^{edge} (at $U/\gamma_0 = 1$) is due to a finite diameter of a tube. (d) The corresponding LDOS curve when $U = \gamma_0$ in (c). The peak structure is sensitive to the position of E_F .

localized edge states have $p_n = \pm 1$ at a unit cell of the edge site and the energy is given by $-\gamma_n$, we see that $\mathcal{H}_{\text{nnn}} = -\gamma_n |p_n|$. Thus, the p_n dependent energy density at a unit cell of the edge site, $\mathcal{H}_U + \mathcal{H}_{\text{nnn}} = (U/8)p_n^2 - \gamma_n |p_n| + \dots$, may become a negative value when the ground state shows a pseudo-spin order, $\langle p_n \rangle \neq 0$. In fact, in the case of $\gamma_n = 0.2\gamma_0$, the magnetization disappears even for $U \approx \gamma_0$.

In Fig. 5(c), we plot P_m^{edge} (solid curve) and P_n^{edge} (dashed curve) as a function of U/γ_0 for $\gamma_n = 0.2\gamma_0$ with $E_F = -0.1\gamma_0$. The results show that, the critical U value decreases as compared with the case of $E_F = 0$ shown by the blue curves in Fig. 5(a). The corresponding LDOS curve for $U = \gamma_0$ is plotted in Fig. 5(d). We see that there are one sharp peak and a broaden peak. Although $P_m^{\text{edge}} \gg P_n^{\text{edge}}$ when $U = \gamma_0$, this two peaks structure is not so clear as the two peaks in the case of $E_F = 0$ with $\gamma_n = 0.1\gamma_0$.

4. Continuous Model

To understand the edge magnetism in detail, we solve eq. (7) analytically by means of a continuous model. It will be shown that the magnetic order is explained by a gauge field for the edge states and spin-dependent mass term.

The low energy states around $E_F = 0$ consist of electrons near the K-point and K'-point. Since the K-point and K'-point are related to each other by time-reversal symmetry, it is sufficient to consider only the K-point when $\mathbf{B}^{\text{em}} = 0$. Then, the low energy Hamiltonian is given by replacing \mathcal{H}_{0s} in eq. (7) with \mathcal{H}_K as

$$\begin{aligned}\mathcal{H}_\uparrow &= \mathcal{H}_K + \frac{U}{4}(\langle p_n \rangle - \langle p_m \rangle)\sigma_z - \frac{U}{4}\langle m \rangle I, \\ \mathcal{H}_\downarrow &= \mathcal{H}_K + \frac{U}{4}(\langle p_n \rangle + \langle p_m \rangle)\sigma_z + \frac{U}{4}\langle m \rangle I,\end{aligned}\quad (9)$$

where \mathcal{H}_K is given by

$$\mathcal{H}_K \equiv v_F \boldsymbol{\sigma} \cdot (\hat{\mathbf{p}} + \mathbf{A}^q(\mathbf{r})), \quad (10)$$

and $\langle n \rangle$ which is present in eq. (7) is dropped in eq. (9) because it can be absorbed in the energy. In eq. (9), \mathcal{H}_s ($s = \uparrow, \downarrow$) operates on a two-component wavefunction, $\psi_s^K = {}^t(\psi_{A,s}^K, \psi_{B,s}^K)$, where $\psi_{A,s}^K$ and $\psi_{B,s}^K$ are the pseudo-spin up and down states, respectively. In eq. (10), v_F is the Fermi velocity, $\hat{\mathbf{p}} \equiv (\hat{p}_x, \hat{p}_y)$ is the momentum operator, and $\boldsymbol{\sigma} \equiv (\sigma_x, \sigma_y)$ where σ_i ($i = x, y, z$) are the Pauli matrices. $\mathbf{A}^q(\mathbf{r}) = (A_x^q(\mathbf{r}), A_y^q(\mathbf{r}))$ is a deformation-induced gauge field that represents a lattice deformation in the hexagonal unit cell [see eq. (8)].^{18,24} The corresponding deformation-induced magnetic field, $B_z^q(\mathbf{r}) \equiv \partial_x A_y^q(\mathbf{r}) - \partial_y A_x^q(\mathbf{r})$, couples to the pseudo-spin, σ_z . This is shown by \mathcal{H}_K squared,

$$\mathcal{H}_K^2 = v_F^2 \{ (\hat{\mathbf{p}} + \mathbf{A}^q(\mathbf{r}))^2 + \hbar B_z^q(\mathbf{r}) \sigma_z \}, \quad (11)$$

where σ_z selects the direction opposite to $B_z^q(\mathbf{r})$ in order to decrease the energy.

In the following, we obtain the wavefunction and the energy eigenvalue E for the following Hamiltonian:

$$(\mathcal{H}_K + m_s \sigma_z) \psi_{p_x, s}^K(\mathbf{r}) = E \psi_{p_x, s}^K(\mathbf{r}), \quad (12)$$

where the mass term is given by

$$m_s \equiv \frac{U}{4}(\langle p_n \rangle \mp \langle p_m \rangle). \quad (13)$$

The mass term depends on real spin, that is, the negative (positive) sign in front of $\langle p_m \rangle$ is for $s = \uparrow$ (\downarrow). Equation (12) describes Dirac fermion having a mass, m_s , where the dimension of m_s is energy here. In obtaining eq. (12), we neglect $\mp(U/4)\langle m \rangle$ of eq. (9). The neglected term does not couple to the pseudo-spin and only shifts the energy position of each state so that it is not important for our discussion. Further, we neglect the \mathbf{r} dependence of m_s in order to simplify the argument.

Since there is translational symmetry along the edge, the eigenfunction of eq. (12) can be expressed by

$$\psi_{p_x, s}(\mathbf{r}) = N \exp\left(i \frac{p_x}{\hbar} x\right) e^{-G(y)} \begin{pmatrix} e^{+g_s(y)} \\ e^{-g_s(y)} \end{pmatrix}, \quad (14)$$

where $s = \uparrow, \downarrow$, and x (y) is parallel (perpendicular) to the zigzag edge.⁵ The unknown functions, $G(y)$ and $g_s(y)$, and E can be determined by putting eq. (14) into eq. (12). We obtain

$$p_x + A_x(y) + \hbar \frac{d}{dy} g_s(y) = D \cosh(2g_s(y) + f_s), \quad (15)$$

$$\hbar \frac{d}{dy} G(y) = D \sinh(2g_s(y) + f_s), \quad (16)$$

where variables D and f_s are defined respectively as

$$D \equiv \pm \frac{1}{v_F} \sqrt{E^2 - m_s^2}, \quad (17)$$

$$\tanh(f_s) \equiv -\frac{m_s}{E}. \quad (18)$$

Here, we consider a localized wavefunction and put $G(y) = |y|/\xi$ into eq. (16) where ξ is localization length of the edge state and the zigzag edge is located at $y = 0$. Then we get

$$2g_s(y) + f_s = \begin{cases} -\sinh^{-1}\left(\frac{\hbar}{\xi D}\right) & (y < 0) \\ +\sinh^{-1}\left(\frac{\hbar}{\xi D}\right) & (y > 0). \end{cases} \quad (19)$$

Next, we integrate eq. (15) with respect to y from $-\xi_g$ to ξ_g . By considering $\xi_g \rightarrow 0$, only singular functions of $A_x^q(y)$ and eq. (19) around $y = 0$ survive, and we get

$$-\sinh^{-1}\left(\frac{\hbar}{\xi D}\right) = \int_{-\xi_g}^{\xi_g} A_x^q(y) dy. \quad (20)$$

Using eqs. (19) and (20), we see from eq. (15) that

$$D = \frac{p_x}{\cosh\left(\int_{-\xi_g}^{\xi_g} A_x^q(y) dy\right)} \quad (21)$$

holds except very close to the edge. From eqs. (20) and (21), we see that ξ in $G(y)$ is given by

$$\frac{\hbar}{\xi} = -p_x \tanh\left(\int_{-\xi_g}^{\xi_g} A_x^q(y) dy\right). \quad (22)$$

This result is surprising in the sense that ξ in the presence of U is identical to ξ for $U = 0$.⁵ The mass term would affect ξ , but it is not the case. The reason for this will be discussed elsewhere. Finally, we get the energy eigenvalue from eqs. (17) and (21),

$$E^2 = m_s^2 + \frac{(v_F p_x)^2}{\cosh^2\left(\int_{-\xi_g}^{\xi_g} A_x^q(y) dy\right)}. \quad (23)$$

The energy dispersion relation for the edge states of eq. (23) is similar to the relativistic energy dispersion relation for the extended state, $E^2 = m_s^2 + (v_F p_x)^2$.

In eq. (18), we see that the sign of f_s depends both on the signs of m_s and E . To obtain a ground state, we first consider the valence states $E < 0$. Then, we have $f_s = \text{sign}(m_s)|f_s|$. Using eq. (20), we can rewrite eq. (19) as

$$g_s(y) = \begin{cases} +\frac{1}{2} \int_{-\xi_g}^{\xi_g} A_x^q(y') dy' - \frac{1}{2} \text{sign}(m_s)|f_s| & (y < 0) \\ -\frac{1}{2} \int_{-\xi_g}^{\xi_g} A_x^q(y') dy' - \frac{1}{2} \text{sign}(m_s)|f_s| & (y > 0). \end{cases} \quad (24)$$

By putting eq. (23) into eq. (18), we have $|f_s| \approx |\int_{-\xi_g}^{\xi_g} A_x^q(y) dy|$ when $|\int_{-\xi_g}^{\xi_g} A_x^q(y) dy| \gg 0$. Since $\int_{-\xi_g}^{\xi_g} A_x^q(y) dy \gg 0$ for the zigzag edge [see Fig. 2(a)], we get from eq. (24)

$$g_\uparrow(y) \approx \begin{cases} \int_{-\xi_g}^{\xi_g} A_x^q(y') dy' & (y < 0) \\ 0 & (y > 0), \end{cases} \quad (25)$$

when $m_\uparrow < 0$. The wavefunction of this spin up state appears near the edge consisting of A-atoms ($y < 0$) in the valence

band ($E < 0$): $\psi_{p_x, \uparrow}(y < 0) \propto \exp(-|y|/\xi)(1, 0)$. The wavefunction at the edge consisting of B-atoms ($y > 0$) is pseudo-spin unpolarized and the amplitude is negligible due to the normalization of the wavefunction. Similarly, for $m_{\downarrow} > 0$, we have

$$g_{\downarrow}(y) \approx \begin{cases} 0 & (y < 0) \\ -\int_{-\xi_g}^{\xi_g} A_x^q(y') dy' & (y > 0). \end{cases} \quad (26)$$

The corresponding wavefunction of spin down state is pseudo-spin down state appearing only near the edge consisted of B-atoms ($y > 0$). It is noted that the spin for a conduction edge state ($E > 0$) is opposite to that of a valence edge state. Thus, we obtain local ferrimagnetism near the zigzag edge.

In Fig. 6, we show how the magnetism appears around the zigzag edge. In Fig. 6(a), if $U = 0$, the opposite direction of pseudo-spin (the edge state) appears both for $y > 0$ ($\sigma_z = -1$) and $y < 0$ ($\sigma_z = 1$). However when $U \neq 0$, due to the mass term the edge state exists only one of the two sides in Fig. 6(a). When pseudo-spin order is suppressed ($\langle p_n \rangle = 0$) and antiferromagnetic order appears ($\langle p_m \rangle \neq 0$), we get a situation of a different sign for m_{\uparrow} and m_{\downarrow} ($m_{\uparrow} = -m_{\downarrow}$) from eq. (13). In this case, up (down) spin edge state appears for $y < 0$ ($y > 0$) for the valence band according to eqs. (25) and (26), while down (up) spin edge state appears for $y < 0$ ($y > 0$) for the conduction band. It is consistent with the numerical result of Fujita *et al.* for $E_F = 0$,⁴⁾ in which the electrons are occupied only for the valence band. If E_F is shifted from $E_F = 0$ then $\langle p_m \rangle$ will disappear.

When pseudo-spin order appears ($\langle p_n \rangle \neq 0$) and antiferromagnetic order is suppressed ($\langle p_m \rangle = 0$), we get another situation that the sign of m_{\uparrow} and m_{\downarrow} are the same ($m_{\uparrow} = m_{\downarrow}$) from eq. (13). In this case, the energy levels for up and down spin edge states are degenerate even for $U \neq 0$ [see Fig. 6(c)]. Thus the ground state is not spin polarized but pseudo-spin polarized. Even in case that $m_{\uparrow} \neq m_{\downarrow}$, spin up and down edge states both appear below the Fermi level so

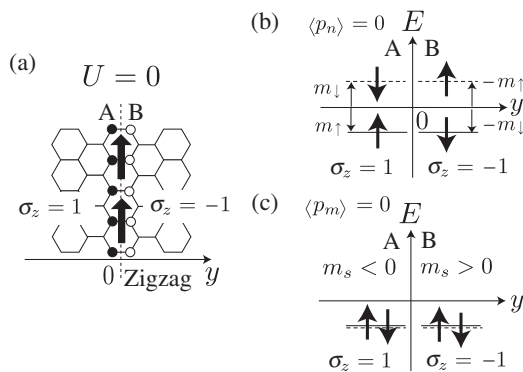


Fig. 6. (a) Deformation-induced gauge (magnetic) field produces asymmetry of pseudo-spin. The pseudo-spin polarized localized state (i.e., the edge states) appears in pair with respect to $y = 0$. (b) Due to the mass term, this symmetric character with respect to $y = 0$ is lost and the edge state can appear independently at $y > 0$ and $y < 0$ (spatial parity with respect to $y \rightarrow -y$ is broken by the mass term). When the sign of the mass is opposite with respect to spin, namely when $m_{\uparrow} = -m_{\downarrow}$, spin becomes asymmetric with respect to $E = 0$, and a local ferrimagnetism appears. (c) In case that $m_{\uparrow} = m_{\downarrow}$, spin up and down states are degenerate and both appear below the Fermi level when $m_s < 0$ ($m_s > 0$) for $y < 0$ ($y > 0$) so that the ground state is spin unpolarized.

that the ground state is still spin unpolarized if $\text{sign}(m_{\uparrow}) = \text{sign}(m_{\downarrow})$. It is interesting to note that, in Fig. 6(c), the energy level position for $y < 0$ can appear above (below) $E_F = 0$ when $m_s > 0$ ($m_s < 0$). The sign of m_s , that is, $m_s < 0$ ($m_s > 0$) for $y < 0$ and $m_s > 0$ ($m_s < 0$) for $y > 0$, is consistent with the numerical results given in §3.

As we have shown in §3, the magnetism of the edge states is affected by the nnn hopping that can stabilize $\langle p_n \rangle$. In the continuous model, we showed in the previous paper that the nnn perturbation works as

$$\mathcal{H}_{\text{nnn}} = \gamma_n \frac{\ell^2}{\hbar} B_z^q(\mathbf{r}) \sigma_z, \quad (27)$$

for the edge states where $\ell \equiv 3a_{cc}/2$.⁵⁾ \mathcal{H}_{nnn} is proportional to σ_z so that \mathcal{H}_{nnn} appears as an additional term for the mass. If γ_n is sufficiently large then we have $m_{\uparrow} = m_{\downarrow}$ and magnetism disappears. This is consistent with the numerical results given in §3.

5. Discussion

A magnetism of the edge states would give rise to two LDOS peaks since only spin up (or down) edge states are located below the Fermi energy to give a spin polarization in the ground state. Although we have examined this mechanism using the Hubbard model, the appearance of two peaks seems to be a model independent consequence of the magnetism of the edge states. The LDOS near the zigzag edge of graphite has been measured by STS,¹¹⁻¹⁵⁾ but no experimental group has observed the two peaks in the STS data. It is possible that the position of the Fermi energy in these experiments is not suitable for the occurrence of the magnetism (see Fig. 5). Thus if we change of the Fermi energy, LDOS will give a split of the peak, which is an evidence that the edge states form a magnetism.

We explained the magnetism of the edge states in terms of the spin dependent mass terms and the deformation induced gauge field. It is known that the mass and a gauge field in the Weyl equation induce the parity anomaly in the ground state.²⁵⁻²⁷⁾ The mass term in eq. (12) changes its sign under spatial parity with respect to $y \rightarrow -y$ and $\psi_{p_x, s}^K \rightarrow \sigma_x \psi_{p_x, s}^K$. The mass term violates the spatial parity and can induce a quantum anomaly in the ground state, which is referred to as the parity anomaly. By applying the formula of the parity anomaly²⁵⁾ to our case, we obtain

$$\langle n_s(\mathbf{r}) \rangle = \frac{1}{2} \frac{B_z^q(\mathbf{r})}{\Phi_0} \text{sign}(m_s) + \dots, \quad (28)$$

where $\Phi_0 = 2\pi\hbar$ is the flux quantum and correction may arise due to higher order derivatives of $B_z^q(\mathbf{r})$. In the case of $m_{\uparrow} = -m_{\downarrow}$, we have magnetism, i.e., $\langle n_{\uparrow}(\mathbf{r}) - n_{\downarrow}(\mathbf{r}) \rangle \neq 0$. Moreover, using $\int_{\text{unit cell}} B_z^q(\mathbf{r}) d^2\mathbf{r} = \pm\Phi_0/4$ that will be derived in the following, the magnetization at the edge is estimated by $\langle m \rangle = \pm 1/4$, which is good agreement with our numerical result, $\langle m \rangle_{0,L} \approx \pm 0.25$, shown in Fig. 4. Thus, we think that there is a close relationship between the edge states magnetism and the parity anomaly. In fact, the anomaly survives even in the massless limit $m_s \rightarrow 0$, which is consistent to the fact that an infinitesimal value of U gives a finite magnetism if we do not consider the nnn interaction [see P_m^{edge} in Fig. 5(a) and Fig. 5 in ref. 4]. A graphene with the zigzag edge and the Klein edge can be used to know that

the deformation induced magnetic field in a unit cell at one side of the edge is given by $\int_{\text{unit cell}} B_z^q(\mathbf{r}) d^2\mathbf{r} = \pm\Phi_0/4$ [see Fig. 2(c)]. In this case, $\Phi^q = \int B_z^q(\mathbf{r}) d^2\mathbf{r}$ is nonzero and the index theorem²⁸⁾ can be used to know $B_z^q(\mathbf{r})$. The theorem states that \mathcal{H}_K possesses $|\Phi^q/\Phi_0|$ zero energy edge states. Since it is known that the number of the zero energy states in a $(n, 0)$ nanotube is given by n ,²⁹⁾ then we can know that the flux in a unit cell at the zigzag edge, Φ_u , is given by $\pm\Phi_0/4$. Here, we used $2 \times (2n\Phi_u) = \pm n\Phi_0$. The factor 2 comes from the time-reversal symmetry (the K and K' points) and the factor $2n$ is the total number of edge sites at the zigzag edge and the Klein edge. $|\Phi_u| = \Phi_0/4$ is consistent with the numerical result by Nakada *et al.*³⁰⁾ who demonstrate that an edge shape with three or four zigzag sites per sequence is sufficient to show an edge state.

In summary, we have shown that the instability of the pseudo-spin order of the edge states induces ferrimagnetic order in the presence of the Coulomb interaction. The nn hopping can stabilize the pseudo-spin order, but a larger value of U makes the pseudo-spin order unpolarized and gives rise to a ferrimagnetic order. The ferrimagnetic order is sensitive to the Fermi energy position. In case that the pseudo-spin order is realized one peak appears in the LDOS near the zigzag edge, which is consistent to the existing experimental results. Using a continuous model of the Weyl equation, we showed that the deformation-induced gauge field gives rise to the magnetism of the edge states if the mass terms have different sign for different spin edge states.

Acknowledgments

Authors would like to thank M. Suzuki and K. Nomura for fruitful discussion. R.S. acknowledges a Grant-in-Aid for Scientific Research (No. 16076201) from the Ministry of Education, Culture, Sports, Science and Technology.

- 1) K. S. Novoselov, A. K. Geim, S. V. Morozov, D. Jiang, M. I. Katsnelson, I. V. Grigorieva, S. V. Dubonos, and A. A. Firsov: *Nature* **438** (2005) 197.
- 2) Y. Zhang, Y.-W. Tan, H. L. Stormer, and P. Kim: *Nature* **438** (2005) 201.
- 3) H. B. Heersche, P. Jarillo-Herrero, J. B. Oostinga, L. M. K. Vandersypen, and A. F. Morpurgo: *Nature* **446** (2007) 56.
- 4) M. Fujita, K. Wakabayashi, K. Nakada, and K. Kusakabe: *J. Phys. Soc. Jpn.* **65** (1996) 1920.
- 5) K. Sasaki, S. Murakami, and R. Saito: *J. Phys. Soc. Jpn.* **75** (2006) 074713.
- 6) K. Sasaki, M. Suzuki, and R. Saito: *Phys. Rev. B* **77** (2008) 045138.
- 7) K. Sasaki, J. Jiang, R. Saito, S. Onari, and Y. Tanaka: *J. Phys. Soc. Jpn.* **76** (2007) 033702.
- 8) S. Okada and A. Oshiyama: *J. Phys. Soc. Jpn.* **72** (2003) 1510.
- 9) K. Kusakabe and M. Maruyama: *Phys. Rev. B* **67** (2003) 092406.
- 10) Y.-W. Son, M. L. Cohen, and S. G. Louie: *Nature* **444** (2006) 347.
- 11) Z. Klusek, Z. Waqar, E. A. Denisov, T. N. Kompaniets, I. V. Makarenko, A. N. Titkov, and A. S. Bhatti: *Appl. Surf. Sci.* **161** (2000) 508.
- 12) Y. Kobayashi, K. Fukui, T. Enoki, K. Kusakabe, and Y. Kaburagi: *Phys. Rev. B* **71** (2005) 193406.
- 13) Y. Kobayashi, K. Fukui, T. Enoki, and K. Kusakabe: *Phys. Rev. B* **73** (2006) 125415.
- 14) Y. Niimi, T. Matsui, H. Kambara, K. Tagami, M. Tsukada, and H. Fukuyama: *Appl. Surf. Sci.* **241** (2005) 43.
- 15) Y. Niimi, T. Matsui, H. Kambara, K. Tagami, M. Tsukada, and H. Fukuyama: *Phys. Rev. B* **73** (2006) 085421.
- 16) T. Ando, T. Nakanishi, and R. Saito: *J. Phys. Soc. Jpn.* **67** (1998) 2857.
- 17) T. Ando: *J. Phys. Soc. Jpn.* **74** (2005) 777.
- 18) K. Sasaki, Y. Kawazoe, and R. Saito: *Prog. Theor. Phys.* **113** (2005) 463.
- 19) D. J. Klein: *Chem. Phys. Lett.* **217** (1994) 261.
- 20) D. Klein and L. Bytautas: *J. Phys. Chem. A* **103** (1999) 5196.
- 21) R. Saito, G. Dresselhaus, and M. Dresselhaus: *Physical Properties of Carbon Nanotubes* (Imperial College Press, London, 1998).
- 22) K. Sasaki, S. Murakami, and R. Saito: *Appl. Phys. Lett.* **88** (2006) 113110.
- 23) D. Porezag, T. Frauenheim, T. Köhler, G. Seifert, and R. Kaschner: *Phys. Rev. B* **51** (1995) 12947.
- 24) C. L. Kane and E. J. Mele: *Phys. Rev. Lett.* **78** (1997) 1932.
- 25) G. W. Semenoff: *Phys. Rev. Lett.* **53** (1984) 2449.
- 26) R. Jackiw: *Phys. Rev. D* **29** (1984) 2375.
- 27) A. N. Redlich: *Phys. Rev. D* **29** (1984) 2366.
- 28) R. A. Bertlmann: *Anomalies in Quantum Field Theory* (Oxford University Press, Oxford, U.K., 2000).
- 29) K. Sasaki, S. Murakami, R. Saito, and Y. Kawazoe: *Phys. Rev. B* **71** (2005) 195401.
- 30) K. Nakada, M. Fujita, G. Dresselhaus, and M. S. Dresselhaus: *Phys. Rev. B* **54** (1996) 17954.